

Journal Name

Crossmark

PAPER

RECEIVED

dd Month yyyy

REVISED

dd Month yyyy

When Blinking Helps: Suppressed Biexciton Emission in Lead Halide Perovskite Quantum Dots

Adam Olejniczak¹ , Jehyeok Ryu^{2,3} , Francesco Di Stasio¹ , Yury Rakovich^{3,4,5,*}  and Victor Krivenkov^{3,5,*} ¹Photonic Nanomaterials, Istituto Italiano di Tecnologia, Via Morego 30, Genova 16163, Italy²Donostia International Physics Center (DIPC), Donostia-San Sebastián 20018, Spain³Polymers and Materials: Physics, Chemistry and Technology, Chemistry Faculty, University of the Basque Country (UPV/EHU), Donostia—San Sebastián 20018, Spain⁴IKERBASQUE, Basque Foundation for Science, Bilbao 48013, Spain⁵Centro de Física de Materiales (CFM-MPC), Donostia - San Sebastián, 20018, Spain

* Authors to whom any correspondence should be addressed.

E-mail: yury.rakovich@ehu.eus (YR) and victor.krivenkov@ehu.eus (VK)**Keywords:** Quantum emitter, Perovskite nanocrystals, Quantum dots, Photoluminescence blinking, Single-photon purity**Abstract**

Blinking and multiphoton emission in metal halide perovskite quantum dots (PQDs) limit their use as single-photon quantum emitters. Conventional models distinguish between trion-related A-type blinking and defect-assisted BC-type blinking, both expected to degrade single-photon purity in a dark state. Here, time-resolved spectroscopy on individual PQDs reveals a qualitatively different regime in which low emitting dark states exhibit higher single-photon purity than bright states. For those PQDs state-resolved $g^{(2)}(\tau)$ analysis shows that the exciton photoluminescence quantum yield decreases by a factor of ~ 8 , while the biexciton one is suppressed by a factor of ~ 10 . This leads to a moderate improvement of single-photon purity with $g_0^{(2)}$ decreased from 0.155 to 0.120. In contrast, PQDs with fluorescence lifetime–intensity distribution patterns characteristic for A-type blinking, display the expected increase of $g_0^{(2)}$ in charged, trion-dominated states. To explain the observed improvement of single-photon purity of low-emitting dark states, we propose a self-trapped-exciton (STE) mechanism that selectively blocks biexciton formation by diverting hot excitons into long-lived, weakly emissive STE configurations. This STE-mediated blinking channel explains why certain low-emitting states improve, rather than degrade, single-photon purity and suggests a lattice-driven route to perovskite quantum emitters with intrinsically suppressed multiphoton events.

1 Introduction

Single-photon emitters are a key resource for quantum communication, computation, and metrology. [1] A central figure of merit is the zero-delay value of the second-order correlation function, $g_0^{(2)}$, which quantifies the probability of emitting more than one photon per excitation event. Values $g_0^{(2)} \ll 0.5$ are required for high-purity single-photon operation.[2]

Colloidal semiconductor quantum dots (QDs) are attractive single-photon sources because they can be processed from solution and integrated into a wide range of photonic architectures.[3] Lead halide perovskite QDs (PQDs) are particularly promising: they exhibit high photoluminescence (PL) quantum yields (QYs), fast radiative rates and broad spectral tunability, and they demonstrate bright single-photon emission at room temperature.[4, 5] At the same time, PQDs suffer from pronounced PL intermittency (blinking) and biexciton emission. Both effects can degrade single-photon performance: blinking reduces the fraction of time the emitter is bright, whereas biexciton emission leads to multi-photon events that increase $g_0^{(2)}$.[6, 7]

The single-exciton PL QY (η_X) is strongly influenced by nonradiative processes due to trap-assisted recombination and trion formation, while the biexciton PL QY (η_{BX}) is predominantly limited by Auger-like processes, in which the recombination energy of one

electron–hole pair is transferred to another hot carrier.[6, 8] Under weak pulsed excitation, when the average number of excitons per pulse $\langle N \rangle \ll 1$, the intrinsic zero-delay correlation of a single PQD can be expressed as $g_0^{(2)} \approx \eta_{BX}/\eta_X$.[6] This relation implies that any blinking mechanism that reduces η_X without a comparable change in η_{BX} will increase $g_0^{(2)}$ in low-emitting (dark) states.

Several distinct blinking mechanisms have been identified in QDs.[9, 10, 11, 12, 13, 14, 15, 16, 17, 18, 19, 20, 21] In A-type blinking, a charge carrier is trapped, and subsequent excitation produces a trion instead of a neutral exciton.[10] The trion PL QY is strongly reduced by fast Auger recombination, while the charged biexciton QY is often suppressed less dramatically.[8, 22, 23] In this case, the ratio η_{BX}/η_X increases in dark blinking states, and $g_0^{(2)}$ is larger than in the neutral bright blinking state, as observed in II–VI and perovskite systems.[24, 25, 18] In band-edge carrier (BC-type) blinking, the PL intermittency is attributed to fluctuating nonradiative rates of band-edge carriers, for example, due to activation and deactivation of shallow traps or surface states.[11, 13, 26, 19, 20] In the simplest BC picture, these fluctuations primarily affect η_X , while η_{BX} remaining controlled by intrinsic Auger processes.

Identification of a blinking mechanism present in an individual QD is usually done by analyzing the correlation between emission intensity and lifetime known as fluorescence lifetime-intensity distribution (FLID) maps.[12, 13]. For BC-blinking, emission intensity is linearly proportional to lifetime, while Auger-type blinking is characterized by nonlinear correlation. Often both A-type and BC-type blinking coexist within one QD.[27, 28, 26, 29, 13, 25, 14] Both mechanisms, however, participate in degradation of single-photon purity in the dark state [25, 18]. Therefore, understanding the relationship between blinking behavior and single-photon purity is critical for advancing PQDs as reliable single-photon sources.

The present work shows a blinking behavior in PQDs, where dark blinking states are not only dimmer and faster than bright states, but also have better single-photon purity, with reduced $g_0^{(2)}$. This behavior cannot be accounted for by any conventional blinking model. Instead, it suggests that, in some cases, blinking in PQDs is controlled by an additional nonradiative channel that suppresses biexciton emission stronger than single-exciton emission.

2 Materials and methods

2.1 *PQD synthesis and ensemble characterization*

Ni-doped CsPbBr₃ PQDs were prepared by ligand-assisted reprecipitation under ambient conditions, following the procedure described in Ref. [30]. This type of nanocrystals was chosen due to their unique long-term PL stability.[30] The Ni-to-Pb molar ratio was $\approx 0.39\%$.[30] For more details about the synthesis see the corresponding section in the Supplementary Information. Transmission electron microscopy (TEM) reveals near-cubic nanocrystals with an average edge length of ~ 10 nm (Figure 1a). The PL and absorption spectra of the PQD dispersion are shown in Figure 1b: the PL peak is centered at 2.46 eV, in agreement with the expected band-edge emission. The PL decay of the PQD solution (Figure 1c) is well described by a biexponential function with an amplitude-weighted average lifetime of 10.4 ns. Additional details about the measurement conditions and the analysis of the time-resolved data are provided in the Supplementary Information.

2.2 *Thin-film samples and single-particle characterization*

For single-particle measurements, 5 μL of the PQD stock solution was mixed with 395 μL of a 1 wt% PMMA solution in anhydrous toluene. A volume of 400 μL of this mixture was dispensed onto a cover glass to fully wet the surface and then spin-coated at 1000 rpm for 60 s under ambient conditions. The resulting film, containing sparsely distributed PQDs in a PMMA matrix, was used immediately for single-dot experiments.

Single-particle characterization and time-correlated single-photon counting (TCSPC) were performed using a MicroTime 200 fluorescence microscope in a Hanbury Brown–Twiss (HBT) configuration under pulsed excitation at 405 nm (repetition rate 5 MHz, pulse width ~ 200 ps). The average exciton occupancy per pulse was kept below 0.1. Emission was collected using a 60 \times water-immersion objective (NA = 1.2), spectrally filtered around the band-edge PL and directed either to a spectrometer or to two avalanche photodiodes for TCSPC and $g^{(2)}(\tau)$ measurements. Most PL decays were non-monoexponential and were fitted by a biexponential function; the effective PL lifetime was then obtained as the amplitude-weighted average lifetime. The instrument response function of the setup was approximately 200 ps.

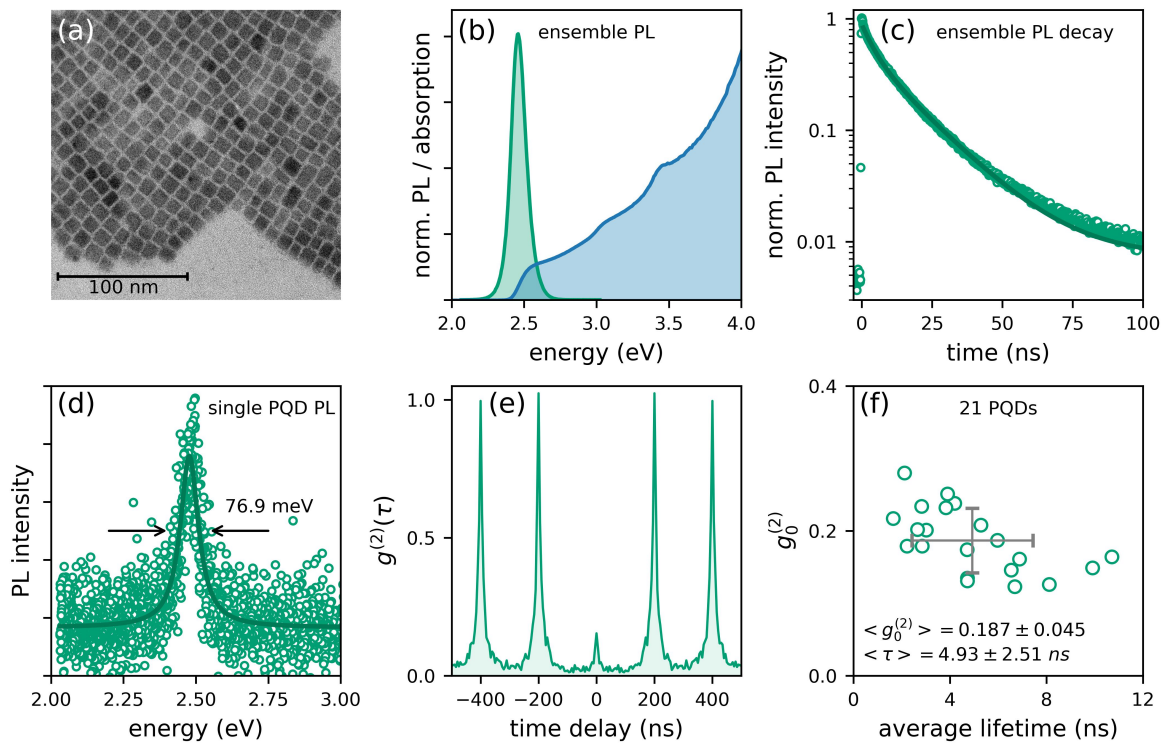


Figure 1. Properties of ensemble (a-c) and single (d-f) PQDs. (a) Representative TEM image of PQDs. (b) Normalized PL and absorption spectra of the PQDs ensemble in solution at room temperature. (c) Ensemble PL decay with a biexponential fit. (d) Emission spectrum of a representative single PQD at room temperature with Lorentzian fit. (e) Representative all-photon second-order correlation function $g^{(2)}(\tau)$. (f) All-photon $g_0^{(2)}$ as a function of average PL lifetime for 21 PQDs at room temperature. Grey cross represents mean values with standard deviations

2.3 Data analysis

Photons emitted from each PQD were divided into 100 ms bins. PL intensity for each bin was calculated as the number of photons per binning time. PL lifetime for each bin was calculated by fitting the decay histogram with a single exponential function for each bin separately. FLID maps were computed as a 2D histogram of PL lifetime and intensity traces. PL decay histograms and second-order correlation functions were calculated for all photons emitted from each PQD, and separately for group of photons selected from the FLID maps, corresponding to bright, intermediate, dark, and trion states. Each PL decay histogram was fitted using biexponential decay function and amplitude average lifetime was calculated separately for each state. Additional details of data analysis are given in Supplementary Information.

3 Results

3.1 General PL parameters of individual PQDs

First, the PL stability of used PQDs was examined. Emission of individual PQDs is characterized by Lorentzian shape with full width at half maximum (FWHM) about 77 meV (Figure 1d). A set of individual PQDs was monitored spectrally for 300 s, and all of them showed stable emission peaks over this interval (Figure S1 in the Supplementary Information). Since the emission wavelength is closely linked to PQD size and electronic structure, the absence of spectral diffusion indicates that no significant structural changes occur on this timescale.^[31] Then, in a TCSPC experiment performed in HBT configuration, 21 individual PQDs from the same ensemble were studied. All of these dots exhibited clear antibunching (Figure 1e) and pronounced PL blinking (see Supplementary Information for details), with a mean single-photon purity $g_0^{(2)} = 0.187$ and mean PL lifetime 4.93 ns (Figure 1f). Thus, under the chosen excitation conditions, PQDs used in the study operate as stable room-temperature single-photon emitters with single-particle spectral width and single-photon purity comparable with previously reported state-of-the-art PQDs.^[32, 4]

Next, the decay kinetics and single-photon purity of PQDs were analyzed separately in bright, intermediate, and dark states. Trion-related photons were analyzed separately when possible. The intensity of trion emission may sometimes be comparable to that of intermediate states in the BC-blinking model.^[25, 13] Selecting bright, intermediate, and dark states based solely on PL

intensity, may lead to mixing of photons originating from intermediate and trion states, thereby hindering the true nature of the emission. Hence, we separated the blinking states by selecting bins within specific ranges of intensity and lifetime on the FLID maps (see Supplementary Information, sections S7 and S8, for details).

Two distinct sub-sets of PQDs could be identified based on how their single-photon purity changes between the bright and dark states. The first sub-set exhibits an improvement or no change in single-photon purity of dark states compared to the bright states, i.e. typically a lower $g_0^{(2)}$, which blinking behavior we refer to as “single-photon blinking” (see Supplementary Information for details). Additionally, these PQDs typically show a linear correlation between PL intensity and lifetime on the FLID map (Figure 2a), forming a line between a bright state (long lifetime, high PL QY) and a dark state (short lifetime, low PL QY). The linear FLID pattern is typical for BC-type blinking; however, a conventional BC model cannot account for the observed improvement of single-photon purity in the dark state (see Supplementary Information for a detailed discussion).

The second sub-set of PQDs displays the opposite trend: the single-photon purity is degraded in the dark-emitting state, with $g_0^{(2)}$ increasing relative to the bright state, which we refer to as “conventional A/BC blinking” (see Supplementary Information for details). These PQDs typically exhibit more complex FLID patterns with both linear and nonlinear components, indicative of the presence of A-type (trion-related) blinking (Figure 3a).

3.2 PL parameters of emission states of PQDs with a single-photon blinking

To demonstrate the effect of single-photon blinking on photon statistics, a representative PQD from this sub-set was selected, showing a clear linear FLID trajectory and no signatures of the trion formation (Figure 2). Three states were defined on the FLID map: a bright state, an intermediate state, and a dark state along the FLID line, marked by a green circle, a yellow diamond, and a blue square in Figure 2a, respectively. The PL decay kinetics of these states are shown in Figure 2b, and the corresponding second-order correlation functions, $g^{(2)}(\tau)$, are displayed in Figures 2c–2e.

For the bright state, the amplitude averaged lifetime is $\tau_B \approx 5.183$ ns and $g_{0,B}^{(2)} \approx 0.248$, giving an exciton QY $\eta_X^B \approx 0.334$ and a biexciton QY $\eta_{BX}^B \approx 0.083$. We estimated the PL QY of the bright state using the assumption that in the biexponential fitting of the PL decay kinetics measured from the stock solution, the long-lifetime component (15.5 ns) is equal to the radiative recombination path of our PQDs, while the short-lifetime component is attributed to the states with nonradiative recombination pathways. For the intermediate state, both averaged lifetime τ_I and $g_{0,I}^{(2)}$ decrease slightly to the values 4.096 ns and 0.199, respectively, corresponding to $\eta_X^I \approx 0.264$ and $\eta_{BX}^I \approx 0.053$. For the dark state, the lifetime is strongly reduced to $\tau_D \approx 1.048$ ns, together with a further decrease of $g_{0,D}^{(2)}$ to ≈ 0.077 , yielding $\eta_X^D \approx 0.068$ and $\eta_{BX}^D \approx 5.2 \times 10^{-3}$.

Thus, when going from the bright to the dark state, the exciton QY decreases by a factor $\frac{\eta_X^B}{\eta_X^D} \approx \frac{0.334}{0.068} \approx 4.9$, whereas the biexciton QY decreases by more than an order of magnitude, $\frac{\eta_{BX}^B}{\eta_{BX}^D} \approx \frac{0.083}{0.0052} \approx 16$. Therefore the ratio η_{BX}/η_X and hence $g_0^{(2)}$ decrease by approximately a factor of three.

In total, we identified 9 QDs (43% of all analyzed in this study) showing reduced $g_0^{(2)}$ values at the dark state. Their $g_0^{(2)}$ and average PL lifetime values calculated separately for bright, intermediate, and dark states are summarized in Figure 2f. The mean PL lifetime decreases from 9.134 ± 3.293 ns for bright states, to 6.238 ± 1.691 ns for intermediate states, to 1.139 ± 0.367 ns for dark states. Although mean values $g_0^{(2)}$ decrease only slightly from 0.155 in bright states, to 0.135 for intermediate states, to 0.120 for dark states. Thus, considering the mean values of the PL lifetime and $g_0^{(2)}$, after changing from bright to dark state, η_X reduces by a factor $\frac{\eta_X^B}{\eta_X^D} \approx 8$.

Meanwhile, biexciton QY reduces by a factor $\frac{\eta_{BX}^B}{\eta_{BX}^D} \approx 10$ (Table 1). The dark state is dim and fast, but also has better single-photon purity than the bright state. This is in stark contrast to the behavior reported for CdSe-based QDs[24] and PQDs with A-type blinking,[25] where lower-emission states typically exhibit higher $g_0^{(2)}$ and thus reduced single-photon purity.

3.3 PL parameters of different emission states of PQDs with a conventional A/BC blinking

A second class of PQDs exhibits an increase in $g_0^{(2)}$ values in the dark state and typically nonlinear FLID patterns, characteristic of A-type blinking or mixed A/BC blinking. Figure 3 shows a representative individual PQD. In contrast to the single-photon blinking case, four distinct states can be distinguished in Figure 3a: a bright neutral state with high PL intensity and long lifetime,

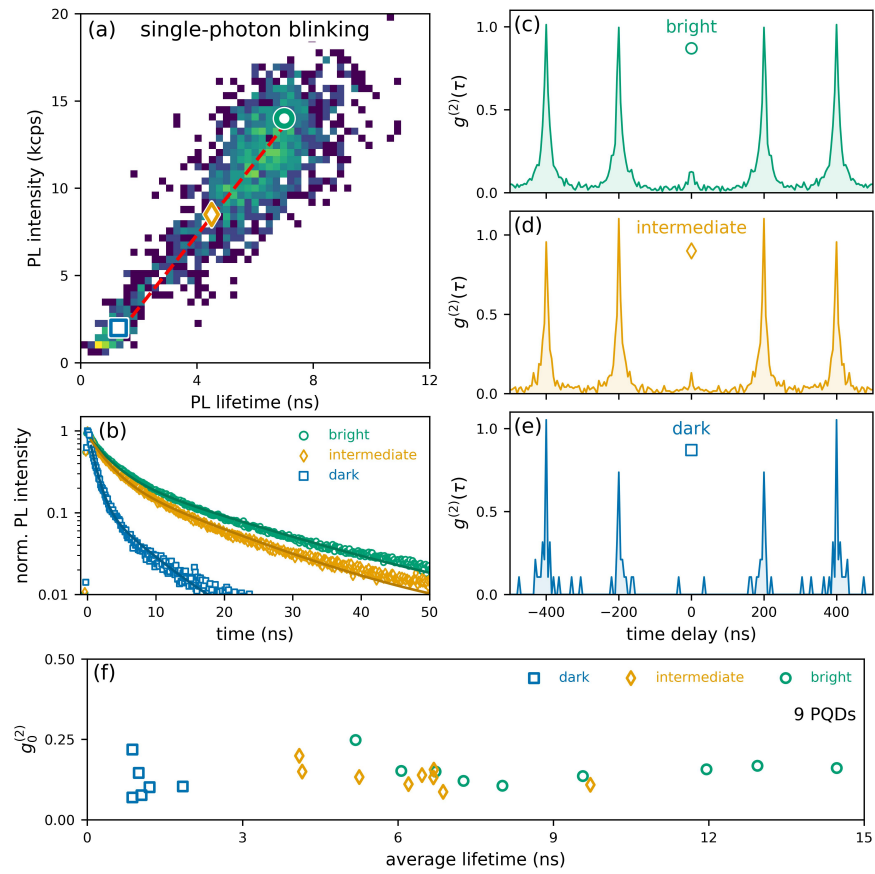


Figure 2. (a-e) PL parameters of different blinking states of individual PQD exhibiting single-photon blinking at room temperature. (a) FLID map with regions corresponding to bright (green circle), intermediate (yellow diamond), and dark (blue square) states. The red dashed line is a guide for the eye. (b) PL decay curves and biexponential fits of bright (green), intermediate (yellow), and dark (blue) states. (c, d, e) State-resolved normalized $g^{(2)}(\tau)$ for the (c) bright, (d) intermediate, and (e) dark states. (f) $g_0^{(2)}$ as a function of average lifetime for bright states (green circles), intermediate states (yellow diamonds), and dark states (blue squares) of 9 PQDs exhibiting single-photon blinking at room temperature.

state	$\langle \tau \rangle$ (ns)	$\langle g_0^{(2)} \rangle$	η_X	reduction	η_{BX}	reduction
bright	9.13 ± 3.29	0.155 ± 0.040	0.59	—	0.091	—
intermediate	6.24 ± 1.69	0.135 ± 0.032	0.40	1.48	0.054	1.67
dark	1.14 ± 0.37	0.120 ± 0.056	0.073	8.08	0.0088	10.34

Table 1. Summary of mean lifetime, $g_0^{(2)}$ and calculated exciton and biexciton QYs for bright, intermediate and dark states of 9 PQDs with single-photon blinking. Reduction is the factor by which exciton and biexciton QY decreased compared to the bright state.

an intermediate state lying on the linear BC-like segment between the bright and dark states, a trion state located on a curved, hyperbola-like trajectory [13] connected to the bright state, and a dark state with the lowest intensity and shortest lifetime.

The PL decays of these states are shown in Figure 3b, and their second-order correlation functions, $g^{(2)}(\tau)$, are presented in Figures 3c-3f. While the bright and intermediate states have similar single-photon purity, with $g_0^{(2)}$ values of 0.174 and 0.168, respectively, the trion state, which has a PL intensity comparable to the intermediate exhibits a substantially higher $g_0^{(2)} \approx 0.35$. The dark state in this PQD also shows degraded single-photon purity with $g_0^{(2)} \approx 0.253$.

For the whole sub-set of PQDs showing the conventional A/BC blinking, the same trend is observed (Figure 3g). The mean $g_0^{(2)}$ of the bright states is 0.194 ± 0.030 , and that of the intermediate states is 0.202 ± 0.042 , with corresponding lifetimes of 5.923 ± 1.749 ns and 3.912 ± 1.588 ns. In contrast, for PQDs where the number of photons sufficient to resolve $g^{(2)}(\tau)$ of the trion state was collected, the mean $g_0^{(2)}$ of the trion state is 0.301 ± 0.061 with a lifetime of 1.457 ± 0.263 ns. The dark states in those PQDs have an even larger mean $g_0^{(2)} = 0.401 \pm 0.151$ and

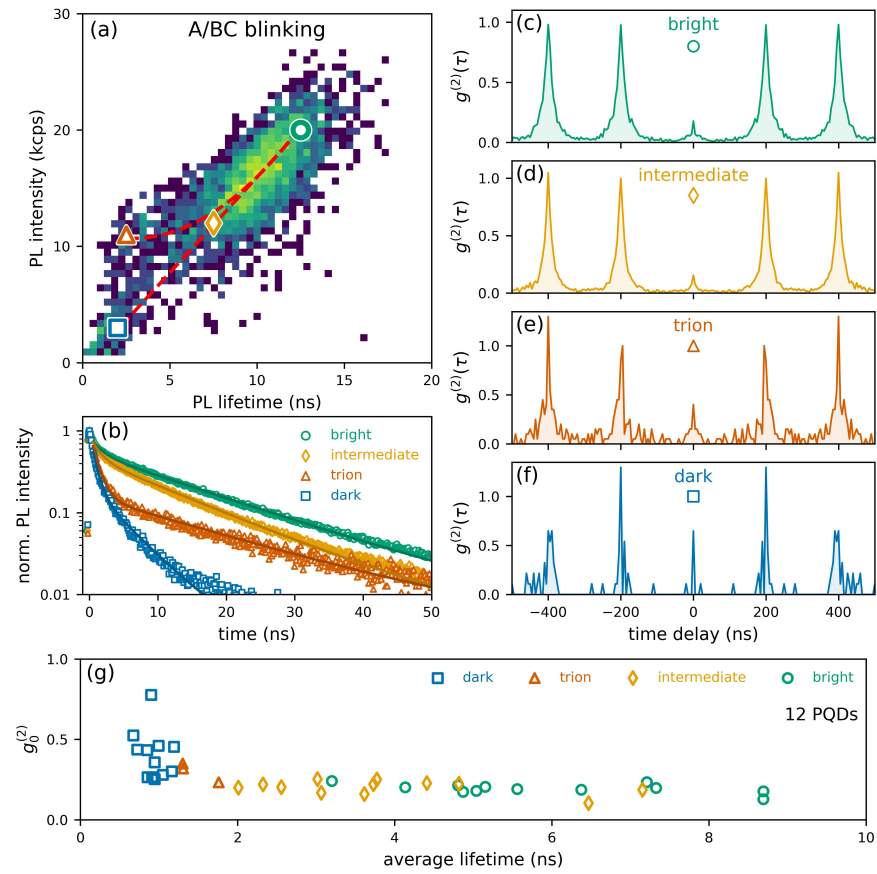


Figure 3. (a-f) PL parameters of different blinking states of individual PQD with a conventional A/BC blinking at room temperature. (a) FLID map with regions corresponding to bright (green circle), intermediate (yellow diamond), trion (red triangle) and dark (blue square) states. Red dashed lines are guides for an eye. (b) PL decay curves and biexponential fits of bright (green), intermediate (yellow), trion (red) and dark (blue) states. (c,d,e,f) State-resolved normalized $g^{(2)}(\tau)$ for the (c) bright, (d) intermediate, (e) trion and (f) dark states. (g) $g_0^{(2)}$ as a function of average lifetime for bright states (green circles), intermediate states (yellow diamonds), trion states (red triangles) and dark states (blue squares) of 12 PQDs exhibiting conventional A/BC blinking at room temperature.

a shorter lifetime of 0.933 ± 0.155 ns.

These observations confirm that in the case of conventional A/BC blinking, dark states cause an increased $g_0^{(2)}$ and reduced exciton QY, which is consistent with A-type and BC-type blinking models.[13] Therefore, the combination of FLID patterns and state-resolved $g_0^{(2)}$ analysis provides a robust means of separating different blinking patterns in PQDs.

4 Discussion

The single-particle measurements on CsPbBr_3 PQDs reveal two qualitatively distinct regimes of intensity intermittency. In the presence of the A-type (trion formation) regime, intensity drops are accompanied by an increase of the zero-delay second-order correlation $g_0^{(2)}$, consistent with blinking driven by trion formation, as it was reported for both II-VI QDs and PQDs.[24, 25] In contrast some of our PQDs display a reduction of $g_0^{(2)}$ in dark blinking states, i.e., an improvement of single-photon purity. These dark states are therefore dimmer and faster than the bright states, yet have better single-photon purity, a behavior that cannot be explained by the conventional BC-type and A-type blinking models. Indeed in the conventional models, based on the formation of trion or short-living defect states, the reduction of η_X should always be stronger than the reduction of η_{BX} (see Supplementary Information file for detailed explanation).

Under the present excitation conditions, corresponding to an average exciton occupancy $\langle N \rangle < 0.1$, the intrinsic zero-delay correlation of a single PQD can be related to the exciton and biexciton quantum yields by the Nair relation $g_0^{(2)} \approx \eta_{BX}/\eta_X$ in the limit $\langle N \rangle \ll 1$.[6] Combining this relation with the radiative lifetime $\tau_{\text{rad}} \approx 15.5$ ns, extracted from the PL decay kinetics of the stock PQD solution, allows both η_X and η_{BX} to be determined for each blinking state via $\eta_X^{(s)} = \tau_s/\tau_{\text{rad}}$ and $\eta_{BX}^{(s)} = g_{0,s}^{(2)} \eta_X^{(s)}$, where term (s) is attributed to one of the states: "B" for the

bright state, "I" for the intermediate state, "D" for the dark state. For the PQDs exhibiting single-photon blinking, the analysis reveals three distinct blinking states (bright, intermediate and dark) with mean lifetimes $\tau_B \approx 9.13$ ns, $\tau_I \approx 6.24$ ns and $\tau_D \approx 1.14$ ns, and corresponding mean $g_0^{(2)}$ values of 0.155, 0.135 and 0.120, respectively. This yields exciton QYs: $\eta_X^B \approx 0.59$, $\eta_X^I \approx 0.40$ and $\eta_X^D \approx 0.073$, and biexciton QYs: $\eta_{BX}^B \approx 0.091$, $\eta_{BX}^I \approx 0.054$ and $\eta_{BX}^D \approx 8.8 \times 10^{-3}$. For the bright state, $\eta_{BX}^B \approx 0.091$ together with the literature value $k_{r,BX} \approx 4.4 k_{r,X} \approx 0.28$ ns⁻¹[7] implies a biexciton Auger rate $k_{A,BX} \approx 2.8$ ns⁻¹, i.e. biexciton recombination is already strongly dominated by Auger processes. Across the bright–dark trajectory, η_X decreases by a factor of ~ 8 , whereas η_{BX} decreases by more than an order of magnitude (a factor of ~ 10). As a result, the ratio η_{BX}/η_X and hence $g_0^{(2)}$ decrease modestly from 0.155 to 0.120 on average.

This trend is opposite to what is expected in the "trap-only" BC-blinking picture established for II–VI QDs,[13] in which activation of shallow traps primarily increases the neutral-exciton nonradiative rate $k_{nr,X}$ while leaving the η_{BX} essentially fixed by Auger recombination. In such a model η_X decreases, η_{BX} remains nearly constant, and $g_0^{(2)} \propto \eta_{BX}/\eta_X$ must increase in dark states. The observed reduction of $g_0^{(2)}$ therefore indicates that an additional nonradiative mechanism suppresses biexciton emission more strongly than single-exciton emission. In A-type blinking, the increase of $g_0^{(2)}$ arises naturally from Auger recombination in trion states. The trion QY η_T is strongly reduced, while the charged biexciton QY η_{BX^\pm} is only moderately suppressed, and a generalized Nair relation yields $g_0^{(2)} \propto \eta_{BX^\pm}/\eta_T$.[24, 25, 6] This explains why in the A/BC blinking regime, dark/charged states show reduced intensity and increased $g_0^{(2)}$ (Figure 4).

For PQDs demonstrating the single-photon blinking, the evolution of $g_0^{(2)}$ opposite to the conventional models points to a different microscopic origin of blinking. We hypothesize that the nature of single-photon blinking is the formation of self-trapped excitons (STEs), which are known to arise in halide perovskites due to strong electron–phonon coupling and lattice softness, and do not require static disorder in the ground-state lattice.[33, 34, 35, 36, 37, 38] Electron–phonon interaction plays an important role in the optical and kinetic properties of QDs, affecting their blinking behavior [39, 40]. In metal–halide perovskites, STEs form via local lattice relaxation around the photoexcited state. Thus, they are highly localized and are Frenkel-like type, in contrast with Wannier–Mott band-edge excitons, distributed over the nanocrystal volume,[41, 42] leading to STE states that are weakly emissive and long-lived at room temperature compared to the band-edge exciton.[36] The localized nature of STEs also weakens STE–exciton interactions, preventing the formation of biexciton.[43]

It was recently proposed by Mi *et al.* that in some CsPbBr₃ PQDs the origin of blinking can also be related to STE formation.[43] In that work, intensity fluctuations at moderate excitation probabilities per pulse were attributed to a biexciton-like Auger interaction between an exciton and a STE, with the second excitation arriving while the STE remains in the PQD. In this scenario, the band-edge exciton acquires an additional nonradiative decay channel associated with Auger recombination. In our model, we assume that the intrinsic radiative rate $k_{r,X}$ remains essentially unchanged, whereas the total decay rate increases due to STE-related nonradiative processes. This implies that the PL intensity scales approximately as $I_{PL} \propto \eta_X \propto k_{r,X} \cdot \tau$, providing a natural microscopic route to a linear intensity–lifetime correlation in FLID maps when STE-related channels act as additional nonradiative decay pathways for the band-edge exciton. As discussed in detail in the Supplementary Information (section S5), the STE-mediated blinking mechanism proposed here can yield a linear FLID pattern, while at the same time providing a natural explanation for the strong suppression of η_{BX} inferred from our $g_0^{(2)}$ data.

Crucially, STE formation competes directly with biexciton (BX) formation at the level of hot excitons (X'). When two photons are absorbed, and the system is promoted from the ground state $|g\rangle$ to a state $|X', X'\rangle$ with two hot excitons, the biexciton cascade $|g\rangle \rightarrow |X', X'\rangle \rightarrow |BX\rangle \rightarrow |X\rangle \rightarrow |g\rangle$ yields two prompt band-edge photons per excitation cycle only if both hot excitons relax to the biexciton state $|X', X'\rangle \rightarrow |BX\rangle$. If instead one of the hot excitons self-traps, the system evolves into configurations such as $|X, STE\rangle$ or $|STE, STE\rangle$, where at most one delocalized band-edge exciton remains and the STE is long-lived, red-shifted, and largely non-emissive on the measurement timescale. Such cycles, therefore, contribute at most to a single prompt band-edge photon and effectively do not generate a biexciton–exciton two-photon cascade.

A simple two-photon (2 γ) excitation model (Figure 4) can help to demonstrate how the STE-related blinking will affect single-photon purity. Each hot exciton in $|X', X'\rangle$ self-traps with probability p_{ST} or relaxes to the band edge with probability $(1 - p_{ST})$. The probability to form a neutral biexciton is then $P_{|X', X'\rangle \rightarrow |BX\rangle} = (1 - p_{ST})^2$. Once in $|BX\rangle$, the biexciton emits its first

photon with an “intrinsic” PL QY $\eta_{BX}^{(0)} = k_{r,BX}/(k_{r,BX} + k_{A,BX}) \approx 0.09$ (extracted from the bright BC state). The overall probability that a two-photon absorption event produces two detectable band-edge photons in one pulse is therefore

$$P(2\gamma | |X', X' \rangle) = \eta_{BX}^{(0)}(1 - p_{ST})^2,$$

which can be viewed as an effective biexciton PL QY. The ratio of biexciton QYs between BC-dark and bright states is then

$$\frac{\eta_{BX}^D}{\eta_{BX}^B} = \left(\frac{1 - p_{ST}^D}{1 - p_{ST}^B} \right)^2.$$

Using the mean experimental values $\eta_{BX}^B \approx 0.091$ and $\eta_{BX}^D \approx 8.8 \times 10^{-3}$ gives $\eta_{BX}^D/\eta_{BX}^B \approx 0.10$. Assuming a negligible bright-state self-trapping probability ($p_{ST}^B \approx 0$), this relation yields $p_{ST}^D \approx 0.69$. Thus, the increase of the hot-exciton self-trapping probability is sufficient to account quantitatively for the observed ~ 10 -fold suppression of η_{BX}^D .

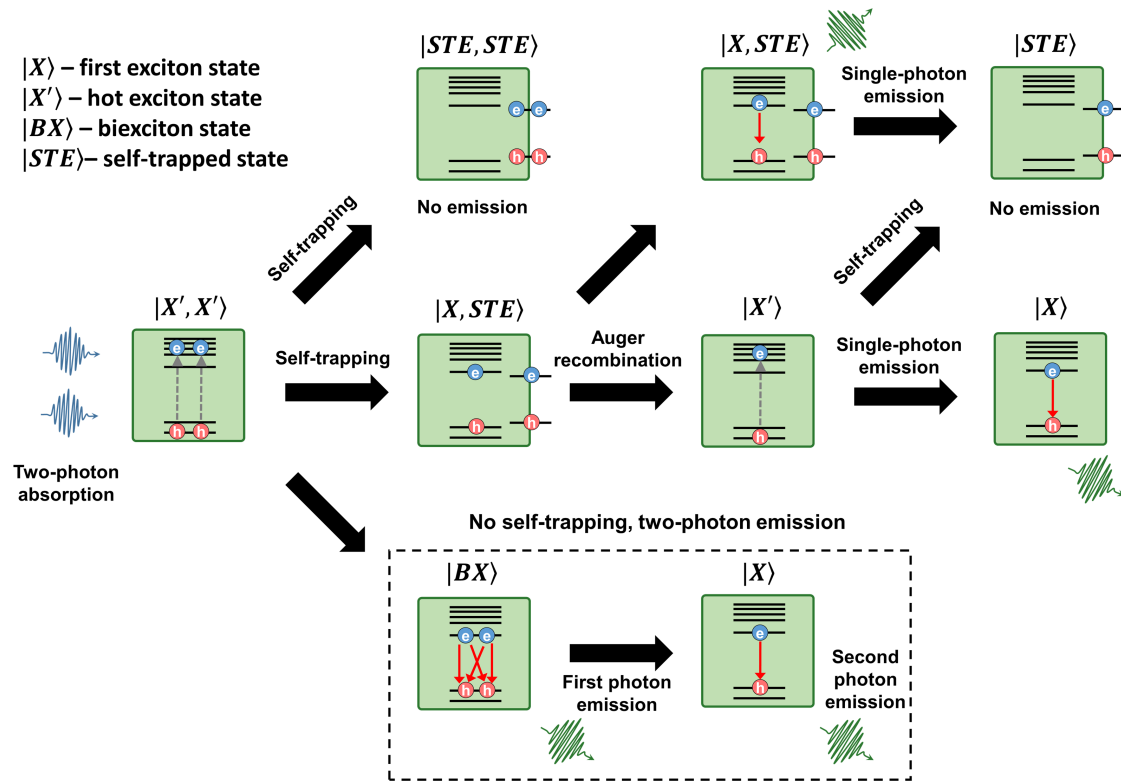


Figure 4. Schematic illustration of the STE-based model explaining suppressed two-photon emission.

Taken together, the data indicate that blinking in CsPbBr_3 PQDs with an improved single-photon purity in the dark states is not merely a perovskite analog of conventional A/BC blinking types in II-VI nanocrystals, but can be contributed by a STE channel that selectively suppresses biexciton emission. In this regime, dark states are dim, fast, and more strongly antibunched than bright states, in contrast to conventional A/BC blinking models. These findings suggest that controlling STE formation and its coupling to band-edge excitons may provide a route to perovskite single-photon sources in which multi-exciton emission is intrinsically suppressed, and highlight the broader role of lattice self-trapping phenomena in defining the quantum-optical response of lead halide perovskites.

5 Conclusions

Ni-doped CsPbBr_3 PQDs were investigated as room-temperature single-photon emitters under weak pulsed excitation. Two distinct blinking regimes were identified at the single-particle level, distinguished by how the single-photon purity changes in the dark emission states. In the first regime, termed “conventional A/BC blinking”, the single-photon purity degraded in the dark emission states, consistent with conventional A/BC blinking models. In the second regime, termed “single-photon blinking”, the FLID pattern is predominantly linear, yet the dark states are not

only dim and fast but also display smaller $g_0^{(2)}$, i.e. improved single-photon purity. Quantitative state-resolved analysis shows that, along this linear FLID trajectory, η_X decreases by a factor of ~ 8 , while η_{BX} decreases by a factor of ~ 10 . As a consequence, the ratio η_{BX}/η_X and hence $g_0^{(2)}$ decrease from 0.155 to 0.120 in the darkest states, opposite to the behavior expected from a trap-only BC blinking model in which η_{BX} is essentially fixed by Auger recombination.

This anomalous trend is explained by a STE-mediated blinking mechanism. In this picture, strong electron–phonon coupling enables the formation of STEs that compete with biexciton formation already at the hot-exciton level. STE-mediated blinking selectively blocks biexciton formation and reduces two-photon emission, while exciton single-photon emission is reduced mainly through additional nonradiative channels. The resulting dark states are therefore simultaneously dim, fast, and have improved single-photon purity with respect to the bright states.

These results identify STE-mediated single-photon blinking as a distinct photophysical pathway in perovskite quantum dots, and demonstrate that this blinking type can, counterintuitively, improve single-photon purity. More broadly, they highlight the role of lattice self-trapping in governing multiexciton dynamics in lead-halide perovskites. Controlling STE formation and its coupling to band-edge excitons may provide a route to perovskite single-photon sources in which multiphoton emission is intrinsically suppressed, and suggests new design strategies for perovskite-based quantum light technologies.

Acknowledgments

Authors acknowledge the financial support by the Department of Science, Universities and Innovation of the Basque Government (grants no. IT1526-22, PIBA_2024_1_0011, and PIBA-2023-1-0007) and the IKUR Strategy; by the Spanish Ministry of Science and Innovation (grants no. PID2022-141017OB-I00, TED2021-129457B-I00, PID2023-146442NB-I00, PID2023-147676NB-I00).

Funding

The study was funded by the Department of Science, Universities and Innovation of the Basque Government (grants no. IT1526-22, PIBA_2024_1_0011, and PIBA-2023-1-0007) and the IKUR Strategy; by the Spanish Ministry of Science and Innovation (grants no. PID2022-141017OB-I00, TED2021-129457B-I00, PID2023-146442NB-I00, PID2023-147676NB-I00).

Author contributions

Adam Olejniczak: Data curation (lead); Visualization (lead); Formal analysis (equal); Writing – review & editing (equal); Conceptualization (supporting); Methodology (supporting); Writing – original draft (supporting). Jehyeok Ryu: Investigation (supporting); Writing – review & editing (equal). Francesco Di Stasio: Funding acquisition (supporting); Supervision (supporting); Writing – review & editing (equal). Yury Rakovich: Funding acquisition (lead); Project administration (supporting); Supervision (supporting); Writing – review & editing (equal). Victor Krivenkov: Conceptualization (lead); Project administration (lead), Methodology (lead); Supervision (lead); Investigation (lead); Writing – original draft (lead); Formal analysis (equal); Writing – review & editing (equal); Visualization (supporting).

Data availability

The data that support the findings of this study are avail from the corresponding author upon reasonable request.

Supplementary data

Details on the PQD synthesis. Details on the PL lifetime measurements. PL stability of individual PQDs. Analysis of the recombinations paths in individual PQDs. Justification of the linear FLID behavior in the STE-based blinking model. STE model for the suppression of the biexciton emission. Details on the analysis of TTTR experimental data. Single PQD datasets: PL intensity and PL lifetime traces, FLID maps, all-photons and state-resolved PL decays with amplitude-weighted lifetimes and second-order correlation functions $g^{(2)}(\tau)$.

References

- [1] Daniel A. Vajner, Lucas Rickert, Timm Gao, Koray Kaymazlar, and Tobias Heindel. Quantum Communication Using Semiconductor Quantum Dots. *Advanced Quantum Technologies*, 5(7):1–40, 2022.

- [2] P Michler, A Imamoğlu, M D Mason, P J Carson, G F Strouse, and S K Buratto. Quantum correlation among photons from a single quantum dot at room temperature . *Nature*, 406(6799):968–970, 2000.
- [3] Adam Olejniczak, Yury Rakovich, and Victor Krivenkov. Advancements and challenges in plasmon-exciton quantum emitters based on colloidal quantum dots. *Materials for Quantum Technology*, 4(3):032001, 2024.
- [4] Young-Shin Park, Shaojun Guo, Nikolay S. Makarov, and Victor I. Klimov. Room Temperature Single-Photon Emission from Individual Perovskite Quantum Dots. *ACS Nano*, 9(10):10386–10393, oct 2015.
- [5] Jehyeok Ryu, Victor Krivenkov, Adam Olejniczak, Alexey Y. Nikitin, and Yury Rakovich. Perovskite nanocrystals as emerging single-photon emitters: Progress, challenges, and opportunities. *Applied Physics Reviews*, 12(4):041323, 12 2025.
- [6] Gautham Nair, Jing Zhao, and Moungi G. Bawendi. Biexciton quantum yield of single semiconductor nanocrystals from photon statistics. *Nano Letters*, 11(3):1136–1140, 2011.
- [7] Bin Li, He Huang, Guofeng Zhang, Changgang Yang, Wenli Guo, Ruiyun Chen, Chengbing Qin, Yan Gao, Vasudevan P. Biju, Andrey L. Rogach, Liantuan Xiao, and Suotang Jia. Excitons and Biexciton Dynamics in Single CsPbBr₃ Perovskite Quantum Dots. *The Journal of Physical Chemistry Letters*, 9(24):6934–6940, dec 2018.
- [8] Nikolay S. Makarov, Shaojun Guo, Oleksandr Isaienko, Wenyong Liu, István Robel, and Victor I. Klimov. Spectral and Dynamical Properties of Single Excitons, Biexcitons, and Triions in Cesium–Lead–Halide Perovskite Quantum Dots. *Nano Letters*, 16(4):2349–2362, apr 2016.
- [9] M. Nirmal, B. O. Dabbousi, M. G. Bawendi, J. J. Macklin, J. K. Trautman, T. D. Harris, and L. E. Brus. Fluorescence intermittency in single cadmium selenide nanocrystals. *Nature*, 383:802, 1996.
- [10] Al. L. Efros and M. Rosen. Random telegraph signal in the photoluminescence intensity of a single quantum dot. *Phys. Rev. Lett.*, 78:1110–1113, Feb 1997.
- [11] Pavel A. Frantsuzov, Sándor Volkán-Kacsó, and Bolízsár Jankó. Model of fluorescence intermittency of single colloidal semiconductor quantum dots using multiple recombination centers. *Phys. Rev. Lett.*, 103:207402, Nov 2009.
- [12] Christophe Galland, Yagnaseni Ghosh, Andrea Steinbrück, Milan Sykora, Jennifer A. Hollingsworth, Victor I. Klimov, and Han Htoon. Two types of luminescence blinking revealed by spectroelectrochemistry of single quantum dots. *Nature*, 479:203, 2011.
- [13] Gangcheng Yuan, Daniel E. Gómez, Nicholas Kirkwood, Klaus Boldt, and Paul Mulvaney. Two Mechanisms Determine Quantum Dot Blinking. *ACS Nano*, 12(4):3397–3405, apr 2018.
- [14] Changgang Yang, Yang Li, Xiaoqi Hou, Mi Zhang, Guofeng Zhang, Bin Li, Wenli Guo, Xue Han, Xiuqing Bai, Jialu Li, Ruiyun Chen, Chengbing Qin, Jianyong Hu, Liantuan Xiao, and Suotang Jia. Conversion of Photoluminescence Blinking Types in Single Colloidal Quantum Dots. *Small*, 20(23):1–12, 2024.
- [15] Changgang Yang, Guofeng Zhang, Jialu Li, Ruiyun Chen, Chengbing Qin, Jianyong Hu, Zhichun Yang, Liantuan Xiao, and Suotang Jia. Mechanisms and Suppression of Quantum Dot Blinking. *Laser and Photonics Reviews*, 19(9):1–18, 2025.
- [16] Cong Tai Trinh, Duong Nguyen Minh, Kwang Jun Ahn, Youngjong Kang, and Kwang Geol Lee. Verification of Type-A and Type-B-HC Blinking Mechanisms of Organic–Inorganic Formamidinium Lead Halide Perovskite Quantum Dots by FLID Measurements. *Scientific Reports*, 10(1):1–8, 2020.
- [17] Vasudevanpillai Biju, Lata Chouhan, Syoji Ito, Elizabeth Mariam Thomas, Yuta Takano, Sushant Ghimire, and Hiroshi Miyasaka. Real-time blinking suppression of perovskite quantum dots by halide vacancy filling. *ACS Nano*, 15(2):2831–2838, 2021.
- [18] Gavin C. Gee, Chenjia Mi, Michael P. LaSala, Wai Tak Yip, and Yitong Dong. Blinking compromises the single-photon purity of individual CsPbBr₃ perovskite nanocrystals. *MRS Communications*, 15(3):391–397, 2025.

- [19] Mrinal Kanti Panda, Debopam Acharjee, Asit Baran Mahato, and Subhadip Ghosh. Hot carrier trapping in light-soaked mixed phase CsPbI_3 perovskite nanocrystals. *Advanced Optical Materials*, 13(10):2402899, 2025.
- [20] Tasnim Ahmed, Sudipta Seth, and Anunay Samanta. Mechanistic investigation of the defect activity contributing to the photoluminescence blinking of CsPbBr_3 perovskite nanocrystals. *ACS Nano*, 13(11):13537–13544, 2019. PMID: 31714741.
- [21] Adam Olejniczak, Ryan Rich, Zygmunt Gryczynski, and Bartłomiej Cichy. Non-excitonic defect-assisted radiative transitions are responsible for new D-type blinking in ternary quantum dots. *Nanoscale Horizons*, 7(1):63–76, 2022.
- [22] Yoshihiko Kanemitsu. Trion dynamics in lead halide perovskite nanocrystals. *Journal of Chemical Physics*, 151(17), 2019.
- [23] Naoki Yarita, Hirokazu Tahara, Toshiyuki Ihara, Tokuhisa Kawawaki, Ryota Sato, Masaki Saruyama, Toshiharu Teranishi, and Yoshihiko Kanemitsu. Dynamics of Charged Excitons and Biexcitons in CsPbBr_3 Perovskite Nanocrystals Revealed by Femtosecond Transient-Absorption and Single-Dot Luminescence Spectroscopy. *The Journal of Physical Chemistry Letters*, 8(7):1413–1418, apr 2017.
- [24] M. Manceau, S. Vezzoli, Q. Glorieux, F. Pisanello, E. Giacobino, L. Carbone, M. De Vittorio, and A. Bramati. Effect of charging on CdSe/CdS dot-in-rods single-photon emission. *Physical Review B*, 90(3):035311, jul 2014.
- [25] Wenli Guo, Jialu Li, Bin Li, Wenzhe Zhang, Changgang Yang, Xue Han, Zhihao Chen, Guangye Yang, Zhichun Yang, Ruiyun Chen, Chengbing Qin, Jianyong Hu, Guofeng Zhang, and Liantuan Xiao. Measurement of absolute biexciton quantum yields in single quantum dots: Breaking the limitation of weak excitation conditions. *Applied Physics Letters*, 127(5), 2025.
- [26] Sudipta Seth, Tasnim Ahmed, and Anunay Samanta. Photoluminescence flickering and blinking of single CsPbBr_3 perovskite nanocrystals: Revealing explicit carrier recombination dynamics. *The Journal of Physical Chemistry Letters*, 9(24):7007–7014, 2018.
- [27] Xue Han, Guofeng Zhang, Bin Li, Changgang Yang, Wenli Guo, Xiuqing Bai, Peng Huang, Ruiyun Chen, Chengbing Qin, Jianyong Hu, Yifei Ma, Haizheng Zhong, Liantuan Xiao, and Suotang Jia. Blinking mechanisms and intrinsic quantum-confined stark effect in single methylammonium lead bromide perovskite quantum dots. *Small*, 16(51):2005435, 2020.
- [28] Taehhee Kim, Seok Il Jung, Sujin Ham, Heejae Chung, and Dongho Kim. Elucidation of photoluminescence blinking mechanism and multiexciton dynamics in hybrid organic–inorganic perovskite quantum dots. *Small*, 15(33):1900355, 2019.
- [29] Jessica Kline, Shaoni Kar, Benjamin F. Hammel, Yumping Huang, Zixu Huang, Seth R. Marder, Sadegh Yazdi, Gordana Dukovic, Bernard Wenger, Henry Snaith, and David S. Ginger. Trion formation hampers single quantum dot performance in silane-coated CsPbBr_3 quantum dots, 2025.
- [30] Jehyeok Ryu, Victor Krivenkov, Adam Olejniczak, Mikel Arruabarrena, Jozef Janovec, Sébastien E Hadjadj, Maxim Ilyn, Aritz Leonardo, Virginia Mart, Andres Ayuela, Alexey Y Nikitin, and Yury Rakovich. Nickel Doping Unlocks Ambient-Condition Photostability in Individual Cesium Lead Bromide Perovskite Quantum Dots. *Nano Letters*, 25(47):16630–16636, 2025.
- [31] Hina Igarashi, Mitsuaki Yamauchi, and Sadahiro Masuo. Correlation between Single-Photon Emission and Size of Cesium Lead Bromide Perovskite Nanocrystals. *Journal of Physical Chemistry Letters*, 14(9):2441–2447, mar 2023.
- [32] Chenglian Zhu, Malwina Marczak, Leon Feld, Simon C. Boehme, Caterina Bernasconi, Anastasiia Moskalenko, Ihor Cherniukh, Dmitry Dirin, Maryna I. Bodnarchuk, Maksym V. Kovalenko, and Gabriele Rainò. Room-temperature, highly pure single-photon sources from all-inorganic lead halide perovskite quantum dots. *Nano Letters*, 22(9):3751–3760, 2022. PMID: 35467890.
- [33] W. Beall Fowler, M. J. Marrone, and M. N. Kabler. Theory of self-trapped exciton luminescence in halide crystals. *Phys. Rev. B*, 8:5909–5919, Dec 1973.

- [34] R. T. Williams, K. S. Song, W. L. Faust, and C. H. Leung. Off-center self-trapped excitons and creation of lattice defects in alkali halide crystals. *Phys. Rev. B*, 33:7232–7240, May 1986.
- [35] Shunran Li, Jiajun Luo, Jing Liu, and Jiang Tang. Self-Trapped Excitons in All-Inorganic Halide Perovskites: Fundamentals, Status, and Potential Applications. *Journal of Physical Chemistry Letters*, 10(8):1999–2007, 2019.
- [36] Bin Yang and Keli Han. Ultrafast Dynamics of Self-Trapped Excitons in Lead-Free Perovskite Nanocrystals. *Journal of Physical Chemistry Letters*, 12(34):8256–8262, 2021.
- [37] Xiaoman Ma, Fang Pan, Haoqi Li, Peng Shen, Chao Ma, Lei Zhang, Haibo Niu, Youzhang Zhu, Shijie Xu, and Honggang Ye. Mechanism of Single-Photon Upconversion Photoluminescence in All-Inorganic Perovskite Nanocrystals: The Role of Self-Trapped Excitons. *Journal of Physical Chemistry Letters*, 10(20):5989–5996, 2019.
- [38] Xiaoxi Wu, M. Tuan Trinh, Daniel Niesner, Haiming Zhu, Zachariah Norman, Jonathan S. Owen, Omer Yaffe, Bryan J. Kudisch, and X.-Y. Zhu. Trap states in lead iodide perovskites. *Journal of the American Chemical Society*, 137(5):2089–2096, 2015. PMID: 25602495.
- [39] Eduard A. Podshivaylov, Maria A. Kniazeva, Alexander O. Tarasevich, Ivan Yu. Eremchev, Andrei V. Naumov, and Pavel A. Frantsuzov. A quantitative model of multi-scale single quantum dot blinking. *J. Mater. Chem. C*, 11:8570–8576, 2023.
- [40] Eduard A Podshivaylov, Aleksandr M Shekhin, Maria A Kniazeva, Alexander O Tarasevich, Elizavaeta V. Sapozhnikova, Anatoly P. Pushkarev, Ivan Yurievich Eremchev, Andrei V. Naumov, and Pavel A Frantsuzov. Model of luminescence and delayed luminescence correlated blinking in single cspbbr₃ nanocrystals. *J. Mater. Chem. C*, pages –, 2025.
- [41] Bogdan M. Benin, Dmitry N. Dirin, Viktoriia Morad, Michael Wörle, Sergii Yakunin, Gabriele Rainò, Olga Nazarenko, Markus Fischer, Ivan Infante, and Maksym V. Kovalenko. Highly emissive self-trapped excitons in fully inorganic zero-dimensional tin halides. *Angewandte Chemie International Edition*, 57(35):11329–11333, 2018.
- [42] Daniele Cortecchia, Jun Yin, Annalisa Bruno, Shu-Zee Alencious Lo, Gagik G. Gurzadyan, Subodh Mhaisalkar, Jean-Luc Brédas, and Cesare Soci. Polaron self-localization in white-light emitting hybrid perovskites. *J. Mater. Chem. C*, 5:2771–2780, 2017.
- [43] Chenjia Mi, Matthew L. Atteberry, Varun Mapara, Lamia Hidayatova, Gavin C. Gee, Madalina Furis, Wai Tak Yip, Binbin Weng, and Yitong Dong. Biexciton-like Auger Blinking in Strongly Confined CsPbBr₃ Perovskite Quantum Dots. *Journal of Physical Chemistry Letters*, 14(23):5466–5474, 2023.